CFD Letters www.cfdl.issres.net Vol. 3 (1) – March 2011

Numerical Evaluation of Inclined Ceiling Diffuser on Buoyancy and Airflow Patterns in an Enclosed Space

Brajesh Tripathi[1C] and Sandipan GhoshMoulic[2]

[1] *School of Packaging, Michigan State University, MI, USA*
[2] *Department of Mechanical Engineering, IIT Kharagpur, WB, India*

Received: 01/10/2010 – Revised 09/11/2010 – Accepted 07/12/2010

Abstract

The effectiveness of an air-conditioning system depends on the airflow pattern inside the room. Expansions in the air conditioning systems by increasing air conditioning capacity or increasing the number of inlets were not an efficient way to achieve comfortable environment. The ideal cooling arrangement usually comes from minimizing the temperature of the air in the mixing zone and then removing the mixed air through the outlet. In the present study, the effect of inlet-outlet configuration on the airflow patterns in a room equipped with a ceiling diffuser was studied. The variation in the direction of incoming air from inlet port was analyzed. A comparison of the various cases showed that the inclination at inlet could be an essential part for the optimum configuration, as the temperature distribution in the occupied zone had least variation. The velocity distribution was almost uniform in most of the occupied zone.

Keywords: Airflow; CFD; Diffuser; Modelling; Buoyancy ratio

1. Introduction

In general, slot type and ceiling type diffusers are employed for creating comfortable environment inside the closed space. In the ceiling type diffusers, air can be diffused with the diffuser mounted on the ceiling at different angles. Ceiling diffusers can be broadly classified as cone, round and square diffuser. In this paper, ceiling type diffusers were analyzed for various inflow and outflow conditions. A newly designed increasing angle type ceiling diffuser was considered in the present investigation.

The two dimensional flow solution of vertical plane diffuser inside the room was well predicted by Nielsen et. al. [1]. They investigated the flow in a rectangular room ventilated by a ceiling plate diffuser for heating and cooling modes using the numerical procedure. The results showed a basic airflow patterns inside the room for limited range of ratio of Grashof number to Reynolds number. Reintarz and Renz [2] investigated the flow in a rectangular room ventilated by a ceiling plate diffuser with flow patterns inside the space. Kato and Murakami [3] provided a method for determining the velocity distribution and spread of contaminants in three-dimensional case for

[C] Corresponding Author: Brajesh Tripathi
Email: brajeshvbn@yahoo.com, Phone – (001)517-432-1431, Fax-(001)517-353-8999
 PII: S2180-1363(11)3148-X

the flow in a clean room. Patel et. al. [4] examined eight different low Reynolds number models and discussed the effect of wall proximity. Awbi and Setrak [5, 6] developed a numerical solution procedure based on Patankar's work to predict the diffusion of isothermal and non-isothermal plane wall jet in rooms. The effect of wall jet diffusion patterns on the opposite wall and air flow rate along the wall was investigated. Awbi [7] solved two and three-dimensional ventilation problems for k-ε turbulence model using finite difference method considering many cases of practical interest.

Murakami et al. [8] analyzed a combination of inflow and outflow conditions on flow diffusion and quality in clean rooms. Chen et. al. [9] predicted natural convection, buoyancy and flow behaviour in cavities using a low Reynolds number k-ε model of turbulence and Boussinesq approximation. Although lots of research conducted to predict two dimensional heat transfer and airflow inside the buildings and initially reported by Nielsen [10]. Nielsen described the suitable k-ε turbulence model for two-dimensional CFD analysis to simulate air movement in a room with proper geometry and boundary condition. Lage et al. [11, 12] reported a transient case of decontaminated environment from their results of a numerical study of a single inlet and outlet from two-dimensional enclosure. Abe et. al. [13] studied turbulent airflow in multi room configuration. Chen and Jiang [14] did a study on the performance of four types of ventilation systems in a classroom with a low ventilation rate. Kato et. al. [15] performed numerical simulation for different cases of flow direction in a room with locally balanced flow rate of air injection system.

William et al. [16, 17] carried out a two part CFD analysis of room air flow implementing the three dimensional Reynolds averaged Navier-Stokes equations for thermal flows in room geometries. Hsu et. al. [18] studied numerically the collective open and strained convection in a moderately separated area with a finite heat source. Davidson and Nielsen [19] studied laminar flow for a backward facing step and low Reynolds number effect and their agreement was found good for experimental data. Calmidi and Mahajan [20] numerically investigated the flow on a heated horizontal surface for a partially open vertical enclosure. They reported their results that a counter balance of the buoyancy driven and forced flow was observed. Hu et.al. [21] presented a CFD study of the indoor environment created through a cold air delivery arrangement with three alternative types of diffusers. Gladstone and Woods [22, 23] investigated the natural convection in a room with a heated floor with laboratory experiments.

Sinha et. al. [24] investigated the velocity and temperature distributions in a two-dimensional room heated by warm air condition. Su et. al. [25] used different alternative modelling to study the circulation of atmospheric air speed, temperature and concentration. Svidt et. al. [26] described the simulation of airflow and temperature distribution in livestock building with different ventilation systems. Their results were visualized by filled contour planes and vector planes in virtual environment. Xu and Chen [27, 28] presented a modified turbulence model for predicting all modes of convection patterns. They used a combination of near wall one-equation and natural convection model and implemented in the direct numerical simulation (DNS). Einberg and Holmberg [29] investigated different flow pattern and air change rates for particle removal efficiency in a ventilated room. Kameel and Khalil [30] introduced a CFD model to predict the air velocity, turbulence level, air temperature and relative humidity distribution in a surgical operating heater. Sun and Smith [31] developed a CFD model with radiation exchange between surfaces to examine the airflow characteristics of a room. Lin and Linden [32] simplified a under floor air distribution system comprising single source of diffuser and heat source for a HVAC system. A lot of work has been carried out to estimate the flow patterns inside the room enclosure at various levels but the flow pattern details were not considered exhaustively, therefore, it was analysed thoroughly in the present work.

2. Numerical details

The Reynolds averaged form of the differential conservation equations of mass, momentum and energy was considered for a scale turbulent motion. Two equation k-ε model was applied to turbulent momentum transport with user defined wall functions. To model the turbulent heat transfer, the Reynolds analogy between heat and momentum transfer was invoked and turbulent Prandtl number Pr_t, which was the ratio of turbulent momentum diffusivity (ν_t) and turbulent thermal diffusivity (α_t), was included in the energy equation. Similarly, to model turbulent mass transfer, Chilton Coleburn analogy was used and turbulent Schmidt number (Sc_t) was included.

2.1. Governing equations

The thermal turbulence modelling proposed by various author offers proper simulation of the thermal field as well as the flow field for complex flows. The following dimensionless variables were used in non-dimensionalized averaged form of governing equations:

$$U_1=\frac{\overline{U_1}}{U_o}, U_2=\frac{\overline{U_2}}{U_o}, U_3=\frac{\overline{U_3}}{U_0},\ X_1=\frac{x_1}{W_1}, X_2=\frac{x_2}{W_1}, X_3=\frac{x_3}{W_1},\ P=\frac{\overline{p}}{\rho U_o^2}, \theta=\frac{\overline{T}-T_o}{T_w-T_o},$$

$$C=\frac{\overline{c}-c_0}{q_s W_1/U_0},\quad \tau=\frac{\overline{\tau}}{W_1/U_o},\quad t^*=\frac{t}{W_1/U_o}, k^*=\frac{k}{U_o^2},\quad \varepsilon^*=\frac{\varepsilon}{U_o^3/W_1},\quad \mu_T{}^*=\frac{\mu_t}{\mu},$$

The resulting mean conservation equations in non-dimensional form can be expressed in the following form (the superscript* and over-score were dropped):

Conservation of Mass (continuity equation)

$$\frac{\partial U_1}{\partial X_1}+\frac{\partial U_2}{\partial X_2}+\frac{\partial U_3}{\partial X_3}=0 \tag{1}$$

Conservation of Xi-Momentum

$$\frac{\partial}{\partial X_j}\left(U_j U_i\right)=-\frac{\partial P}{\partial X_i}+\frac{\partial}{\partial X_j}\left(\left(\frac{1}{\mathrm{Re}}+\frac{\mu_T}{\mathrm{Re}}\right)\left(\frac{\partial U_i}{\partial X_j}+\frac{\partial U_j}{\partial X_i}\right)\right)+\frac{Gr}{\mathrm{Re}^2}\theta\delta_{i,2} \tag{2}$$

Energy conservation equation

$$\frac{\partial U_1\theta}{\partial X_1}+\frac{\partial U_2\theta}{\partial X_2}+\frac{\partial U_3\theta}{\partial X_3}=\frac{\partial}{\partial X_j}\left(\left(\frac{1}{\mathrm{Re\,Pr}}+\frac{\mu_T}{\mathrm{Re\,Pr_T}}\right)\frac{\partial\theta}{\partial X_j}\right) \tag{3}$$

Equation for the Contaminant concentration

$$\frac{\partial U_1 C}{\partial X_1}+\frac{\partial U_2 C}{\partial X_2}+\frac{\partial U_3 C}{\partial X_3}=\frac{\partial}{\partial X_j}\left(\left(\frac{1}{\mathrm{Re\,Sc}}+\frac{\mu_T}{\mathrm{Re\,Sc_T}}\right)\frac{\partial C}{\partial X_j}\right)+S_c^* \tag{4}$$

Equation for the Local mean age

$$\frac{\partial U_1\tau}{\partial X_1}+\frac{\partial U_2\tau}{\partial X_2}+\frac{\partial U_3\tau}{\partial X_3}=\frac{\partial}{\partial X_j}\left(\left(\frac{1}{\mathrm{Re}\,Sc}+\frac{\mu_T}{\mathrm{Re\,Sc_T}}\right)\frac{\partial\tau}{\partial X_j}\right)+1 \tag{5}$$

Equation for Turbulence energy

$$\frac{\partial U_1 k^*}{\partial X_1}+\frac{\partial U_2 k^*}{\partial X_2}+\frac{\partial U_3 k^*}{\partial X_3}=\frac{\partial}{\partial X_j}\left(\left(\frac{1}{\mathrm{Re}}+\frac{\mu_T}{\sigma_k \mathrm{Re}}\right)\frac{\partial k^*}{\partial X_j}\right)+G_k-\varepsilon^*-G_b \quad (6)$$

Equation for the Dissipation rate

$$\frac{\partial U_1 \varepsilon^*}{\partial X_1}+\frac{\partial U_2 \varepsilon^*}{\partial X_2}+\frac{\partial U_3 \varepsilon^*}{\partial X_3}=\frac{\partial}{\partial X_j}\left(\left(\frac{1}{\mathrm{Re}}+\frac{\mu_T}{\sigma_\varepsilon \mathrm{Re}}\right)\frac{\partial \varepsilon^*}{\partial X_j}\right)+\frac{\varepsilon}{k}f_1 C_1 G_k-C_2 f_2 \varepsilon^*+C_3 G_b \quad (7)$$

where δ_{ij} was the Kronecker delta. The values of the different dimensionless numbers were given as:

Dimensionless number	Corresponding value
S_c	1.0
Pr	0.7
Sc_t	0.7
Pr_t	0.8

Here, the Reynolds averaged equations were closed using the two-equation k-ε eddy-viscosity model. Expression of μ_T, G_b and G_k were given as follows

$$\mu_T=\mathrm{Re}\frac{c_\mu f_\mu k^2}{\varepsilon},\quad G_b=\frac{\mathrm{Gr}}{\mathrm{Re}^3}\frac{\mu_T}{\mathrm{Pr}_T}\frac{\partial\theta}{\partial X_2}\qquad G_k=\frac{\mu_T}{\mathrm{Re}}\left(\frac{\partial U_i}{\partial X_j}+\frac{\partial U_j}{\partial X_i}\right)\frac{\partial U_i}{\partial X_j}$$

The damping functions f_μ , f_1 and f_2 for the Lam-Bremhorst (LB [33]) low Reynolds number (LRE) k-ε model used in this investigation were given by

$f_\mu=(1-\exp(-A_\mu R_k))^2\left(1+\frac{A_t}{R_t}\right)$, $f_1 = 1+ (Ac_1/ f_\mu)\ 3$, $f_2 = 1- \exp(-R_{t2})$ where $R_t = \mathrm{Re}\ k^2/\varepsilon$,

$R_k = \mathrm{Re}\ k^{1/2y}$, $A_\mu = 0.0165$, $A_t = 20.5$, $Ac_1 = 0.05$.

2.2. Boundary conditions

This section discussed the boundary conditions used at the solid walls, inlet and outlet. The turbulent kinetic energy and the turbulent dissipation were not required to be specified for the laminar case, as they did not contribute. In Figure 1, the velocity and temperature boundary conditions were specified. Only front, top, bottom and inlet boundaries were shown for simplicity. Different types of boundaries were considered in the present investigation, which includes inflow, outflow and solid wall boundaries. Inlet boundary conditions for a room airflow model were important in obtaining the accurate solution for the computation of ventilation flow with two-equation turbulence models.

The velocities, temperature and turbulent transport quantities over the inlet boundary were usually prescribed either from the experimental data or from pre-calculated distributions. In present investigation velocity, temperature, k, ε, C and τ were assumed uniform at the inlet cross-section and the details were given in Table 1.

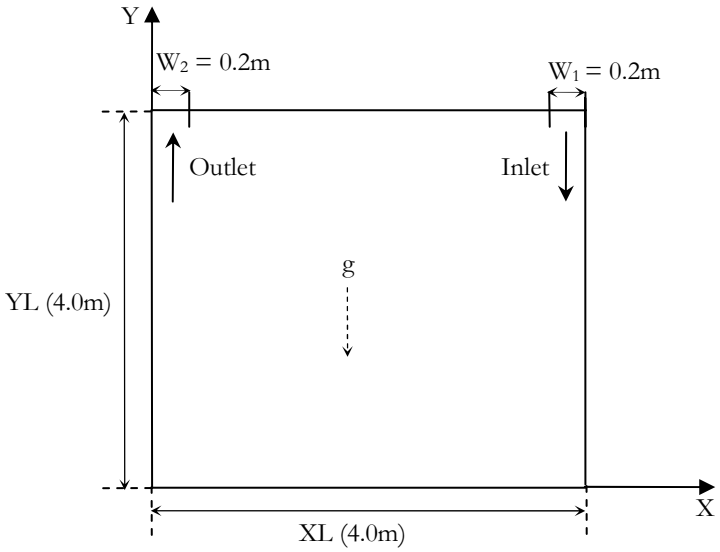

Figure 1: Schematic of Case I showing outlet position on left side of ceiling (all dimensions are in m)

In case of zero inclination of inlet jet, inlet velocity was assumed horizontal ($U_2 = 0$). In the cases of specified inlet angle, both u and v components were specified at the inlet. Compared to the boundary conditions imposed at the walls and the inlet, the outlet boundary conditions were relatively simple. Neumann boundary conditions had been applied for the flow variables at outlet, that was, $\delta\varphi/\delta n = 0$, where n was the direction normal to the outflow boundary. The velocity profile at the outlet was iteratively corrected so as to satisfy the global mass flow rate. All walls in the room were non-porous. Therefore, the normal velocity was always equal to zero. No-slip boundary condition was used at the wall for the U_1, U_2 and U_3 velocity components. $U_1 = U_2 = U_3 = 0$, $\theta = 1$. The boundary conditions for k and ε in the low Re number Lam Bremhorst model were

$$k = 0 \quad \varepsilon = \frac{1}{\mathrm{Re}} \frac{\partial^2 k}{\partial X_3^2} \qquad \text{at top and bottom side} \qquad (8)$$

$$k = 0 \quad \varepsilon = \frac{1}{\mathrm{Re}} \frac{\partial^2 k}{\partial X_2^2} \qquad \text{at ceiling and floor} \qquad (9)$$

$$k = 0 \quad \varepsilon = \frac{1}{\mathrm{Re}} \frac{\partial^2 k}{\partial X_1^2} \qquad \text{at left and right wall} \qquad (10)$$

Neumann boundary conditions were used for species concentration and local mean age of air at the walls. Usually in CFD modelling, the no slip boundary condition was imposed for the nodes inside the boundary layer, if the grid size was larger than the boundary layer thickness, then the slip condition would yield better results. The boundary conditions were summarized in Table 1.

The computational domain shown in fig. 1 had been divided into non-overlapping control volumes. Fine grids were chosen near the walls, inlet and outlet. All the scalar variables were defined at the centre of the control volumes and also located on the boundaries for convenience of specifying the boundary conditions [24]. The discretized equations were obtained by integrating Navier-Stokes and energy equations over the control volumes. SIMPLE and extension of SIMPLE algorithm by Patankar [34] were implemented. The opening of inlet and outlet were enlarged up to the width of the room. Inlet and outlet were located on top of the left

wall and bottom of the right wall, respectively. Flow behaviour was obtained by solving equations in a Fortran Program developed in the laboratory which had a structure of pre, process and post-processor.

TABLE 1: BOUNDARY CONDITION FOR DIFFERENT MODELS

Model	U_1	U_2	U_3	θ	k	ε	C	τ
Laminar Flow								
a. At the wall b. At the inlet	0 1	0 0	0 0	1 0	- 	- 	$\frac{\partial C}{\partial n}=0$ 0	$\frac{\partial \tau}{\partial n}=0$ 0
Turbulent Flow								
(A) HRE (High Reynolds number) model (standard k-ε model)								
a.At the wall b. At the inlet	0 1	0 0	0 0	1 0	0 0.005	$2k/\mathrm{Re}\,y_P^2$ $k^{1.5}/W_1$	$\frac{\partial C}{\partial n}=0$ 0	$\frac{\partial \tau}{\partial n}=0$ 0
(B) LRE (Low Reynolds number) model								
a. At the wall b. At the inlet	0 1	0 0	0 0	1 0	0 0.005	$2k/\mathrm{Re}\,y_P^2$ $k^{1.5}/W_1$	$\frac{\partial C}{\partial n}=0$ 0	$\frac{\partial \tau}{\partial n}=0$ 0

Note: ε at the wall was calculated using the value of k near the wall.

After the grid independence test, verification of the results in the central plane of the room in the third direction was used for comparison. The value of Re at the supply opening was 5000. The computed profiles of horizontal component of mean velocity (u/U_0) and turbulent intensity $I = (\sqrt{\overline{u'^2}}/U_0)$ along the x = 2H were plotted in Figure 1b, along with the corresponding measured results.

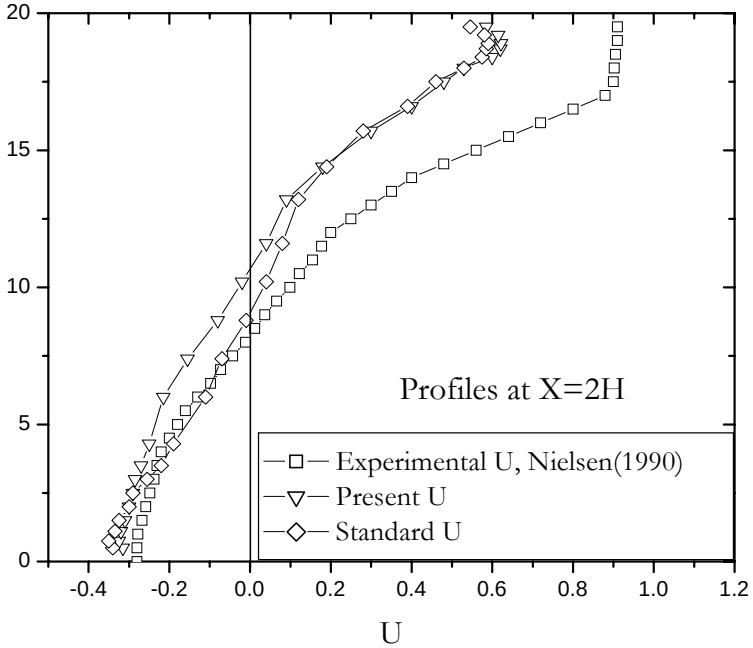

Figure 1b: Computed and measured dimensionless velocity (U) at section x/H=2 with experimental data reported by Nielsen, 1990 [37]

The velocity profiles computed by applying the k-ε (standard) model and the Lam-Bremhorst (LB) low Reynolds number (LRE) k-ε model (present model) were found to be in good agreement with the measurements. However, there were various factors influencing the prediction of simulated results. These factors included selection of the grid spacing and its distribution and location at the near wall region.

3. Results and discussion

In this paper, effect of inlet-outlet configuration on the airflow patterns in a room equipped with a ceiling diffuser was studied. A typical square room of length 4m and height 4m was considered, as shown in Figure 1. The inlet, of width W_1 = 0.2m, was located on the right side of the ceiling and outlet, of width W_2 = 0.2m, was placed on the left side of the ceiling. The air was entered from the right side of the ceiling and exited from the left side of the ceiling. All walls were at a particular constant temperature except at the inlet and outlet. The validation of the results was simulated using benchmark solution by Neilson [10] and presented in a paper Tripathi & GhoshMoulic [35].

A 98 x 92 grid was adopted in X-direction and Y-direction respectively. In boundary layers, very fine grid was chosen near the walls for high quality resolution of results. These grid points were expanded by power law towards the interior of the room. It leaded to a reduction in computation time compared to uniform grid, while yielding a good accuracy. The solution was taken to be converged when the normalized residuals were less than 10^{-4}. The airflow pattern was analyzed, for all the ranges of Re and buoyancy ratio, in terms of streamlines, isotherms, heat-lines and variation in average Nusselt number. All the plots were presented for non-dimensional length of 20, i.e. Dimensional length (4.0m)/inlet width (0.2m) =20. These results were presented for two values of Re, namely 1000 and 2000 for turbulent flows.

Case I & II were defined in Figure 1 with and without inclination inlet. The room geometry for ceiling type diffuser was shown in Figure 1 for Case I. The inlet and outlet slots extended throughout the width of the room in z-direction. The width of the room in the z-direction was assumed to be much larger than 4m. Thus, the flow may be treated as two-dimensional flow. Figures 2 depicted the plots of streamlines and isotherms for Case I at Re=1000 and buoyancy ratios Gr/Re^2 = 0.1 and 0.5. Figure 2 (a) showed the streamline pattern for buoyancy ratio of 0.1. It was indicated that the main air stream entered vertically downward from the inlet. The cold air stream attached with the right wall, travelled a short distance along the right wall, then detached from the right wall, touched the floor, moved upwards along the left wall and left through the outlet situated at the left corner of the ceiling. A big clockwise-rotating recirculatory cell was observed in the central part of the room above the main air stream, covering a large portion of the room. A counter-clockwise rotating cell was formed near the bottom right corner below the main air-jet. Another small counter-clockwise rotating cell of lesser intensity was observed near the bottom left corner, deflecting the flow away from the occupied zone. The main air-jet touched the right wall, floor and left wall as it moved from the inlet to the outlet. Figure 2(b) depicted the isotherms for this flow, at buoyancy ratio of 0.1. Temperature variation was observed in most of the occupied zone, while in the non-occupied zone (upper part of the room), it was almost constant except near the walls.

Figure 2 (c) depicted the streamlines for buoyancy ratio of 0.5, at Re = 1000. The figure showed that when the buoyancy ratio was increased to 0.5, the cold air stream did not stoop straight downward. It was deflected away from the right wall due to the formation of a small vortex near the upper portion of the right wall. Then, the cold air stream touched the floor, moved upwards along the left wall, and went out through the exit port. On increasing the buoyancy ratio, the two small vortices near the bottom left and bottom right corners were eliminated. The size of the big clockwise-rotating recirculatory cell was reduced. The isotherms for buoyancy ratio of 0.5 were

shown in Figure 2 (d). The figure described that the uniformity of temperature in the occupied zone increased with increasing the buoyancy ratio.

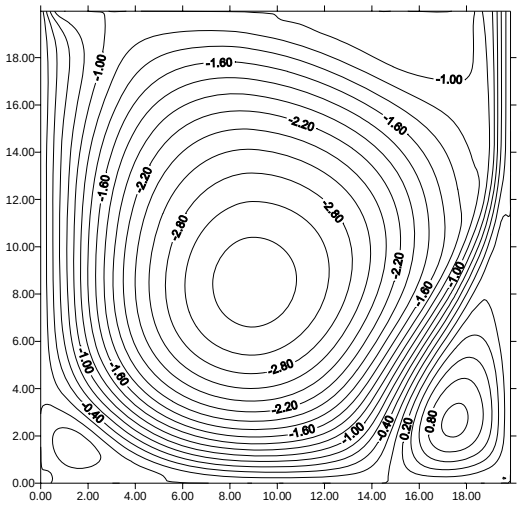

(a) Streamlines for buoyancy ratio = 0.1

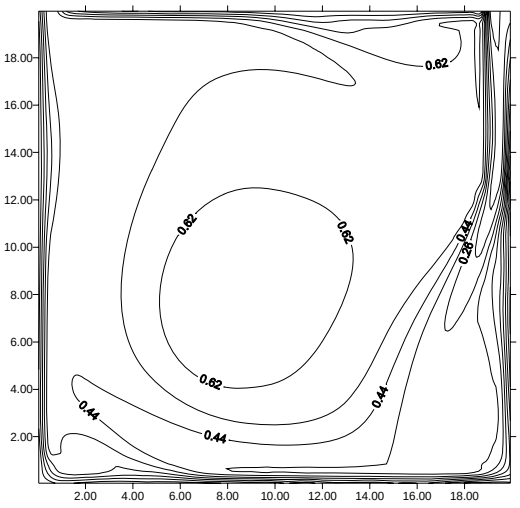

(b) Isotherms for buoyancy ratio = 0.1

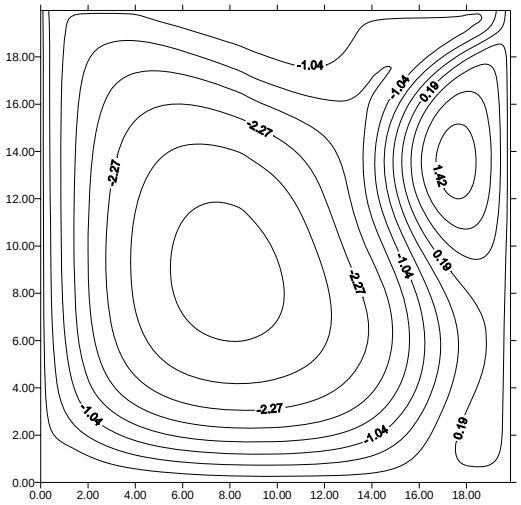

(c) Streamlines for buoyancy ratio = 0.5

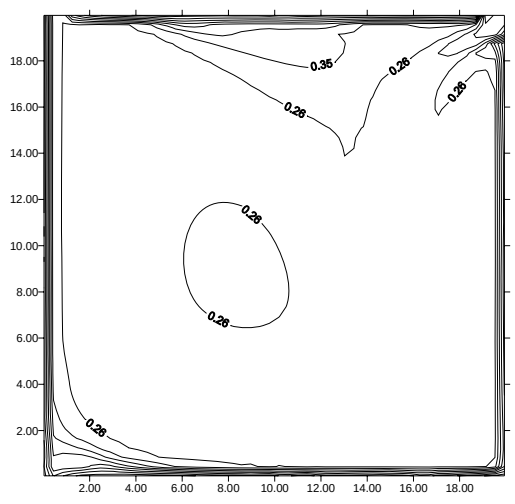

(d) Isotherms for buoyancy ratio = 0.5

Figure 2: Streamlines and isotherms for Case I at Re = 1000

Figure 3 presented contours of streamlines and isotherms at Re = 2000 and buoyancy ratio = 0.1 and 0.5. The streamline contours at Re = 2000 and buoyancy ratio of 0.1 were plotted in Figure 3 (a). As in Figure 2 (a), the main air-stream touched the right wall, floor and left wall as it moved from the inlet to the outlet, Figure 3 (a) showed two counter-rotating vortices on either side of the main air-stream. Increase in the Reynolds number reduced the size of big recirculatory cell above the main air stream, and increased the size of the vortex below the main air stream. Figure 3(b) showed the isotherms for Re = 2000 and buoyancy ratio of 0.1. The figure indicated the temperature variation in the occupied zone.

Figure 3(c) showed the streamlines for Re = 2000 and buoyancy ratio of 0.5. Comparison of figures 3 (a) and (c) indicated that the strength of the counter-clockwise turning recirculatory cell beneath the main air-jet increased with the increase in the buoyancy percentage to 0.5. Figure 3(d) showed the isotherms at Re = 2000 and buoyancy ratio of 0.5. It was showed that increasing the buoyancy ratio to 0.5 resulted in more uniformity in the temperature in the occupied zone.

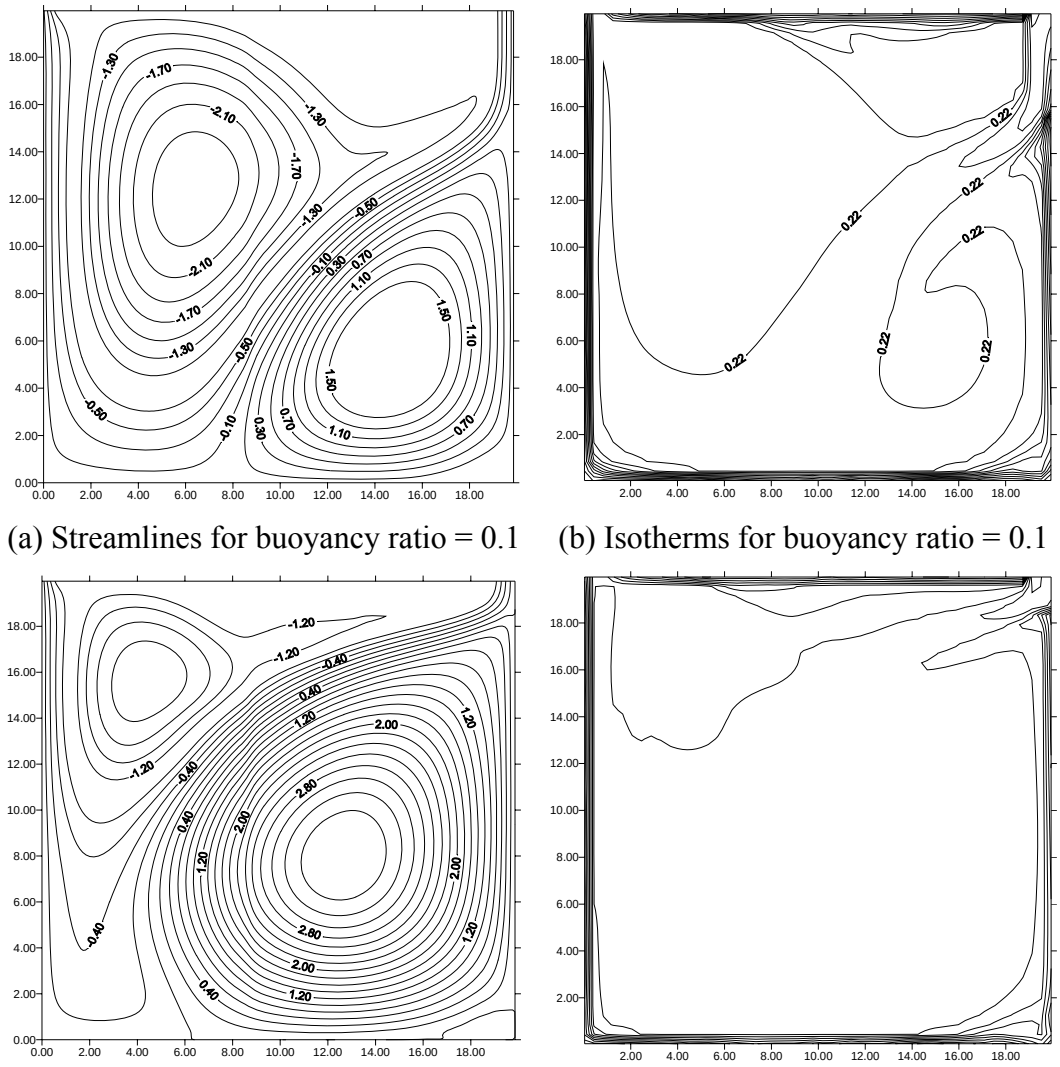

(a) Streamlines for buoyancy ratio = 0.1 (b) Isotherms for buoyancy ratio = 0.1

(c) Streamlines for buoyancy ratio = 0.5 (d) Isotherms for buoyancy ratio = 0.5

Figure 3: Streamlines and isotherms for Case I at Re = 2000

4. Simulation of airflow for inclined inlet jet

The room geometry for ceiling type diffuser was shown in Figure 4 for Case II (Tripathi et. al.[36]). A room of similar dimensions, of length 4m and height 4m was considered. The fresh air entered from the right side of the ceiling and exited from the left side of the ceiling. The side, top and bottom walls were kept at constant temperature that was higher than the temperature of incoming air. The inlet velocity was diffused through a series of vanes as shown in the enlarged part of Figure 4. The inlet width (W_1) was divided into 12 equal intervals. The angle for the first grid point was taken as 5.5^0. The angles for other grid points was increased such that, $\psi_{n+1} = \psi_n + 5.5^0$, where n = 0, 1,…, 11.

Figures 5 showed the streamlines and isotherms for Case II, at Re=1000 and buoyancy ratios of 0.1 and 0.5. The streamlines for Re = 1000 and buoyancy ratio of 0.1 were shown in Figure 5(a). The figure indicated that the inlet stream of cold air went downwards near the right wall up to short distance, recirculated in the room along the left wall and taken through outlet. A huge clockwise turning recirculatory zone was seen in the upper central part of the room. Two small counter-clockwise rotating vortices were observed below the main air-stream, near the bottom left and bottom right corners.

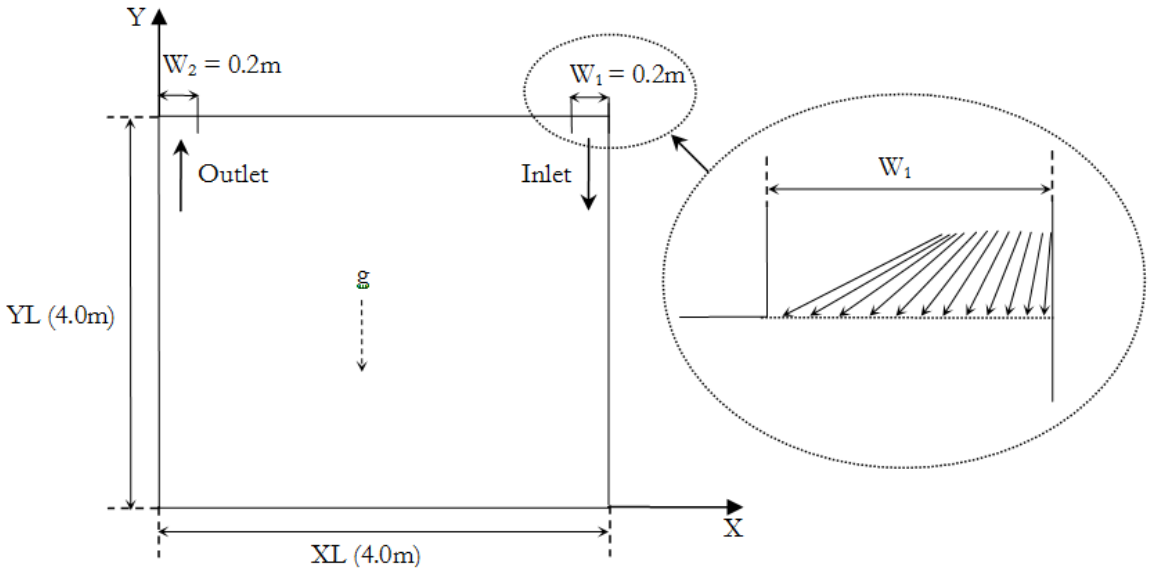

Figure 4: Schematic of Case II (all dimensions are in m)

The comparison of figures 2 (a) and 5 (a) indicated that the two corner vortices near the floor were larger in size, for Case II. This was due to the inclination of the inlet air-jet. In this case, the main air-jet did not touch the floor. The main air-stream was deflected upwards of the floor due to the increase in size of the vortices near the bottom left and bottom right corners. Figure 5 (b) showed the isotherms at Re = 1000 and buoyancy ratio of 0.1. Temperature gradients were seen in the occupied zone.

Figure 5 (c) showed the streamline pattern for Re = 1000 and buoyancy ratio of 0.5. The figures showed that when buoyancy ratio increased to 0.5, the cold air stream did not stoop downwards. It attached with the ceiling, moved along the ceiling up to middle of the room and went vertically downwards. Finally, it attached with the left wall and then exited through outlet. The uniformity of temperature in the occupied zone at the higher buoyancy ratio of 0.5 was found to increase, as shown in Figure 5(d).

Figure 6(a), (b) and (e) showed the streamlines, isotherms and heat-lines at Re = 2000 and buoyancy ratio of 0.1. Figure 6(a) showed that the inlet cold air stream attached with the ceiling for a small space. It went vertically downward in the middle of the enclosure, touched the left wall then taken out through outlet. Figure 6(a) revealed four vortices in the flow field. A large clockwise rotating vortex was seen in the upper central part of the room, as in Figure 5 (a). A counter-clockwise vortex was observed below the main air-jet, occupying a large portion of the region near the floor. Two relatively smaller vortices were seen near the bottom left corner, and in the region of the ceiling to the right of the outlet. Figure 6(b) showed that the temperature variation was largely confined to the thermal boundary layers near the right and left walls. The heat lines in Figure 6 (e) indicated that the cold air stream entered the room and exchanges energy. Maximum values for heat lines were found at the centre of the room. These values were found to be lower in the occupied region. The pattern of heat-lines in Figure 6 (e) was similar in nature to the streamline pattern in Figure 6 (a). This indicated that the energy was transported inside the room mainly by convection along streamlines.

Figure 6 (c), (d) and (f) showed the streamlines, isotherms and heat-lines at Re = 2000 for buoyancy ratio = 0.5. Figure 6(c) showed that the small vortices near the bottom left corner and in the region near the ceiling to the right of the outlet disappeared with the increase in the buoyancy ratio to 0.5. The size of the clockwise-rotating vortex in the upper central part of the room reduced

considerably in size. Figure 6 (d) showed that the uniformity of temperature increased as the value of buoyancy ratio increases.

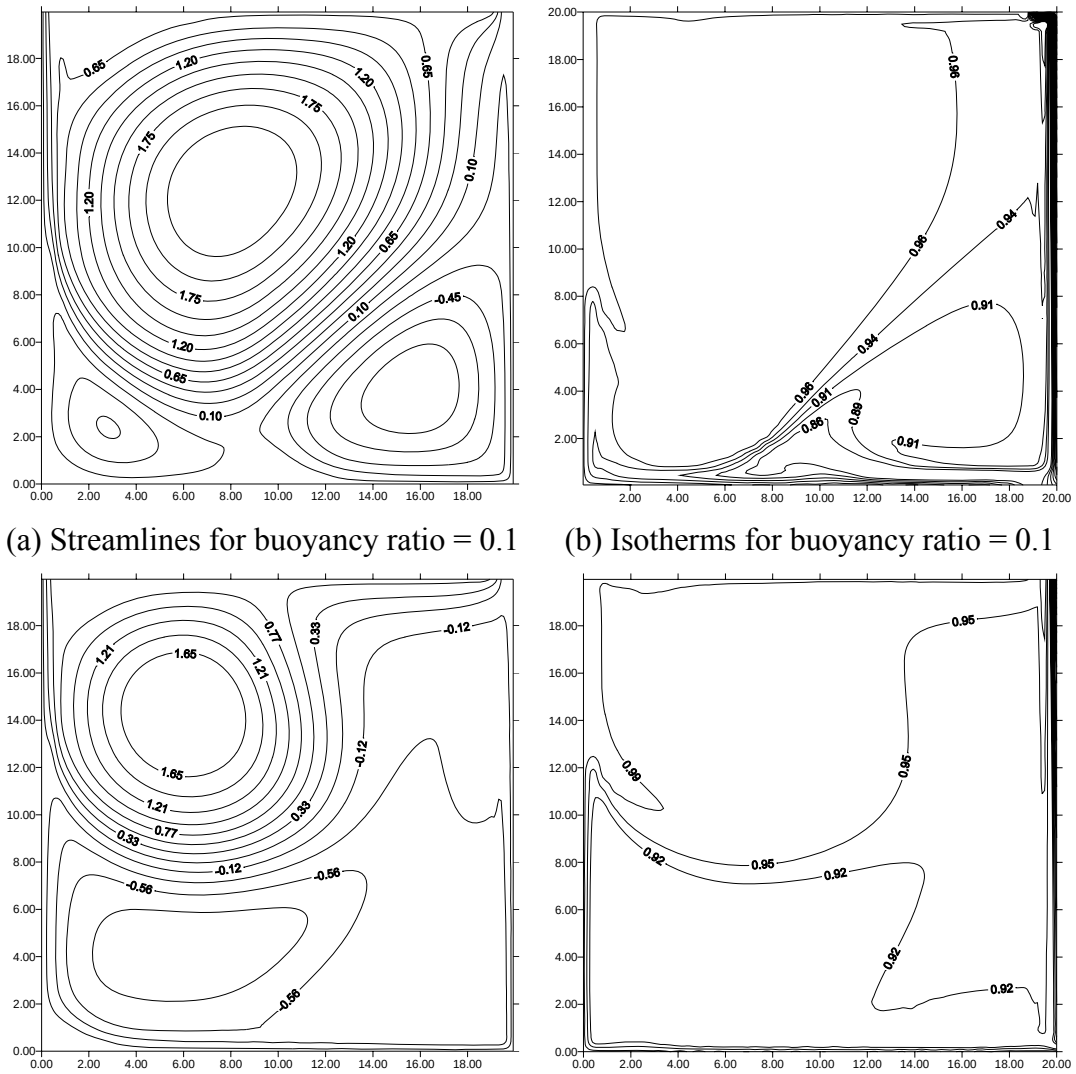

(a) Streamlines for buoyancy ratio = 0.1 (b) Isotherms for buoyancy ratio = 0.1

(c) Streamlines for buoyancy ratio = 0.5 (d) Isotherms for buoyancy ratio = 0.5

Figure 5: Streamlines and isotherms for Case II at Re = 1000

The comparison of Figure 6 (c) and 6 (f) indicated that the patterns of heat-lines and streamlines were almost similar. Lower values of heat function were observed in the occupied zone for higher buoyancy ratios. The streamlines and isotherm pattern of Case II indicated that the variation in the velocity and temperature of incoming air was mostly in the non-occupied zone. Better recirculation in the occupied region was obtained in Case II. Also, temperature variation was lower in the occupied zone in Case II, compared to Case I. A comparison of the average Nusselt numbers on the right and left walls was presented in Figure 7, for Case II and Case I (straight and inclined inlet jet), at Re=1000.

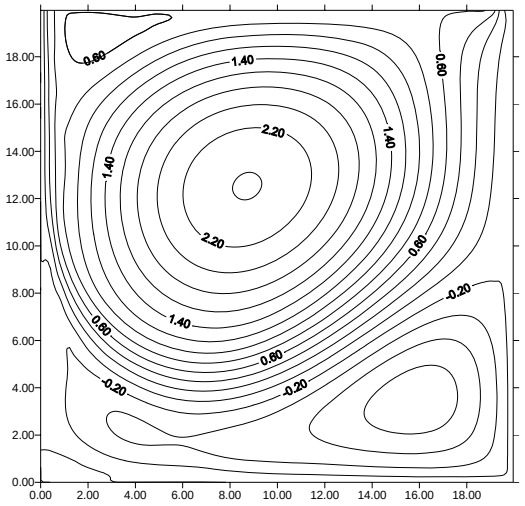

(a) Streamlines for buoyancy ratio =0.1

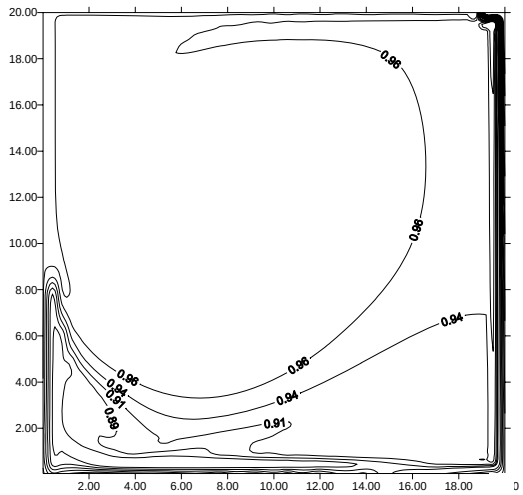

(b) Isotherms for buoyancy ratio=0.1

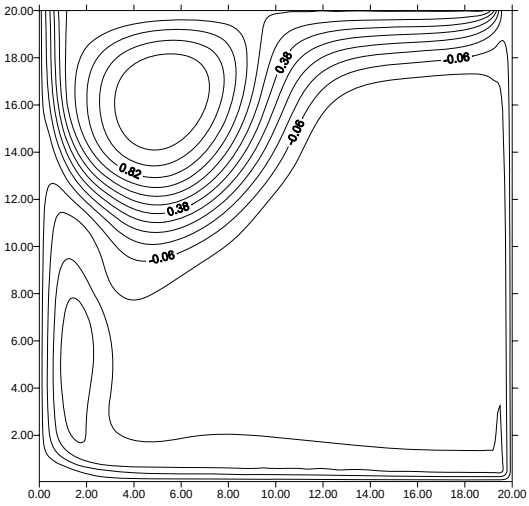

(c) Streamlines for buoyancy ratio =0.5

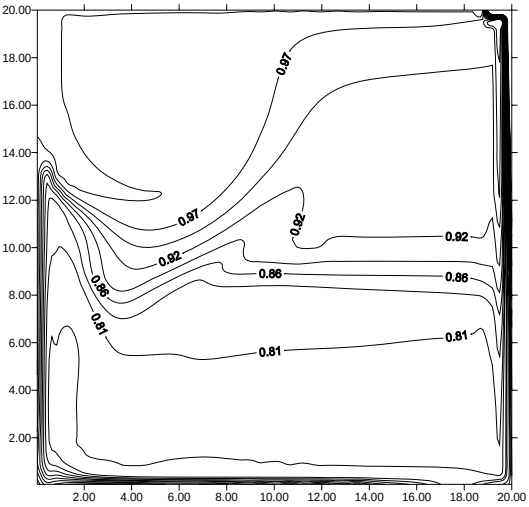

(d) Isotherms for buoyancy ratio=0.5

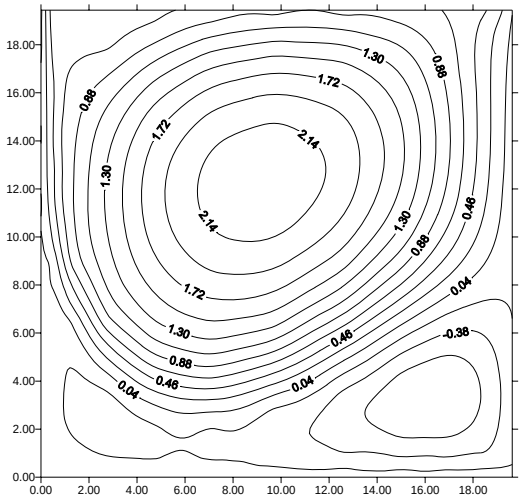

(e) Heat-lines for buoyancy ratio =0.1

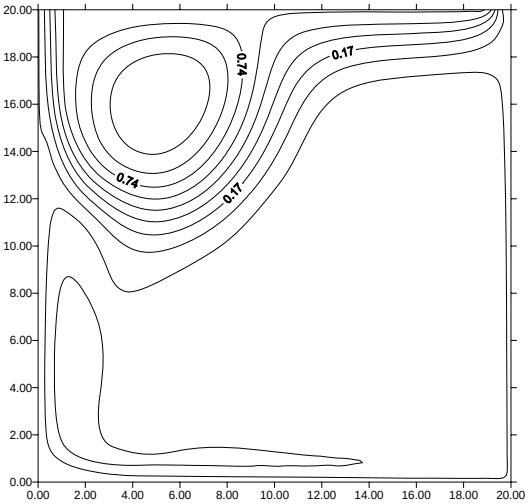

(f) Heat-lines for buoyancy ratio =0.5

Figure 6: Streamline, isotherms and heat-lines for Case II at Re=2000

The average Nusselt number on the right wall was plotted on the left Y-axis, while the average Nusselt number on the left wall was plotted on the right Y-axis. It was observed that with increase in the buoyancy ratio, the average Nusselt numbers on both the walls was increased. Higher values of the average Nusselt number were obtained for Case II. Therefore, the heat transfer was higher on the right and left walls, for Case II. These values were closer for very high buoyancy ratios. The average Nusselt number on the left and right walls were given in Table 2, for different buoyancy ratios. It was observed that the average Nusselt number on right wall increased with the increase in buoyancy ratio. The average Nusselt number on the left wall also increased with the increase in buoyancy ratio but at a slower rate.

The position of the centre of the main clockwise-rotating cell at different buoyancy ratios was given in Table 3. The table indicated that with the increase in the buoyancy ratio, the centre of this vortex moved towards the left wall.

It was observed from the flow pattern analysis that for ceiling type diffusers, inclination created some difference in the flow patterns and at the higher buoyancy ratios, uniform distribution of temperature was observed throughout the occupied zone. This was due to the fact that incoming air was divided into several air streams after coming from the inlet. The left part of incoming air stream was attached with the ceiling while right part of the incoming air stream was attached with the right side wall. At very low buoyancy ratios and low Reynolds number, the incoming air stream was weaker and hence, did not reach the occupied region due to poor recirculation. But at higher buoyancy ratio, the circulation was uniform throughout the room and covered most of the area of the room.

TABLE 2: VARIATION IN THE AVERAGE NUSSELT NUMBERS WITH BUOYANCY RATIOS (Gr/Re^2), FOR CASE II

Reynolds number	Buoyancy ratio (Gr/Re^2)	Nusselt number at right wall	Nusselt number at left wall
1000	0.1	2.92458	1.09051
	0.2	5.06887	1.20561
	0.4	7.91397	1.26927
	0.6	9.67500	1.29847
	0.8	11.1008	1.31818
	1.0	12.3475	1.35037
2000	0.1	3.49232	1.65386
	0.2	6.55938	1.77813
	0.4	10.5120	1.86365
	0.6	12.1275	1.91987
	0.8	16.3919	1.98599
	1.0	19.9164	2.03522

TABLE 3: CENTRE POSITION OF MAIN CIRCULATING CELL FOR CASE II

Buoyancy ratio	Position of the cell (X,Y) for Re = 1000	Position of the cell (X,Y) for Re = 2000
0.1	9.5, 12.25	8.8, 11.2
0.2	8.0, 12.1	7.5, 12.3
0.4	6.8, 13.5	6.2, 15.6
0.6	6.0, 14.0	5.3, 16.9
0.8	5.0, 14.5	4.4, 17.3
1.0	4.0, 16.0	3.7, 17.7
2.0	2.5, 19.0	2.5, 18.2
5.0	1.8, 19.8	1.6, 18.8

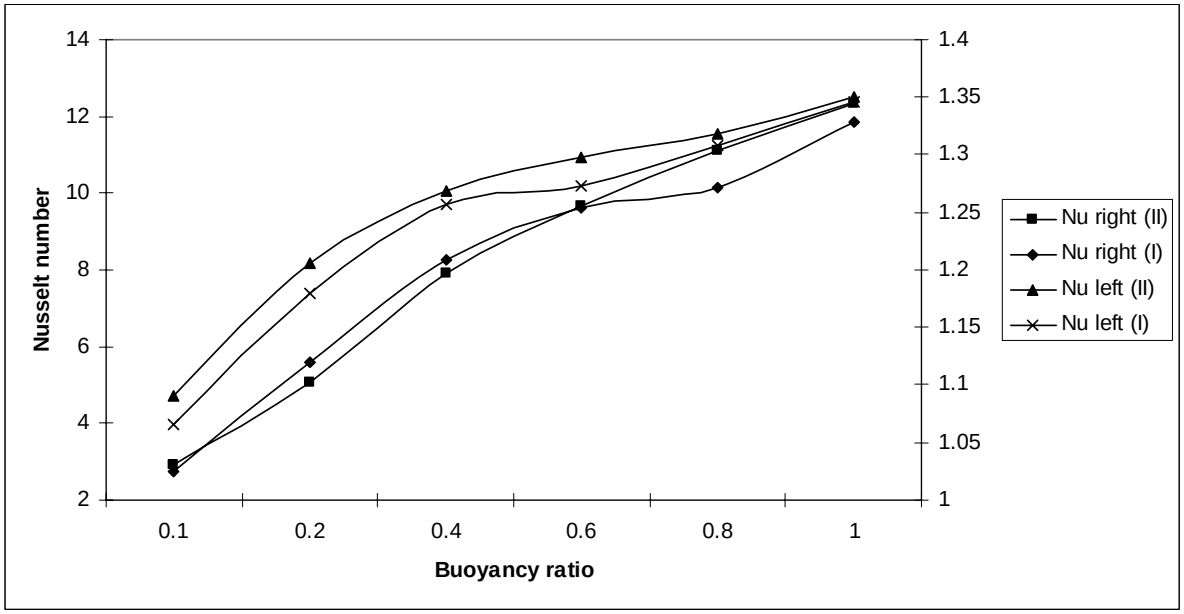

Figure 7: Comparison of Nusselt numbers on right and left walls for Case I and Case II (straight and inclined inlet jet) at Re=1000

5. Conclusion

A Computational Fluid Dynamics simulation was carried out to evaluate the effect of variable inlet inclination and location for the ceiling type diffuser. A two-equation k-ε eddy-viscosity model was used for the weakly induced turbulent jet through the inlet diffusion. A FORTRAN code was prepared in accordance with in house turbulent flow code for the originality of the flow simulation. A detailed comparative study was completed for the grid independence and suitable turbulent model to accurately predict low Re number flow. All the results were compared with the benchmark solution and experimental data to estimate CFD simulation and found to be in good agreement. Two cases of inclination of cold air injection were carried out and results were compared to find the effect of inclination at inlet on room airflow patterns. The important findings were summarized below:

The main circulating cell moved towards the left wall for inclined inlet, Case II. The recirculation, consistency of velocity and temperature in the occupied zone increased with increase in buoyancy ratio. The uniformity of temperature in the occupied zone was higher for the inclined air-jet. Therefore, it can be used for the different configurations of room airflow simulations. Some other aspect ratio can be analyzed for large industrial use and a concentration of various gases presented inside the living room may be considered for the future work.

Nomenclature

Ar	aspect ratio
C	contaminants concentration,
C_0	concentration at the inlet,
Gr	Grashof number,
k	turbulent kinetic energy,
Pr	Prandtl number,
p	pressure of fluid,
Re	Reynolds number,
Sc	Schmidt number,

T_0	inlet temperature,
T_w	wall temperature,
T	Temperature of fluid,
U_0	inlet velocity,
W_1	inlet opening,
W_2	outlet opening,
XL	horizontal distance in X-direction,
YL	vertical distance in Y-direction,
ZL	horizontal distance in Z-direction.

Symbol

ΔT	difference between inlet and wall temperature,
β	coefficient of thermal expansion,
μ	absolute viscosity of fluid,
μ_t	turbulent viscosity,
ν	kinematic viscosity of fluid,
ρ	reference density of the fluid,
ε	dissipation of turbulent kinetic energy,
τ	local age of air,
Γ_Φ	diffusion coefficient,
Φ	general dependent variable.

References

[1] Nielsen P.V., Restivo A. and Whitelaw J.H., The Velocity Characteristics of Ventilated Room, Journal of Fluid Engineering, 1978. 100: p. 291-298.

[2] Reinartz A. and Renz U., Calculations of the Temperature and Flow Field in Room Ventilated by a Radial Air Distributor, Int. J. Refrigeration, 1984. 7: p. 308-312.

[3] Kato S., Murakami S. and Nagano S., Numerical study on diffusion in a room with a locally balanced supply exhaust airflow rate system, ASHRAE transactions, 1992. 98(I): p. 248-257.

[4] Patel V.C., Rodi W. and Scheuerer G., Turbulence models for near wall and low Reynolds number flows: a review, AIAA Journal, 1985. 3: p. 230-239.

[5] Awbi H.B. and Setrak A.A., Numerical Solution of Ventilation Air Jet, 5th Int. Symposium on use of Computers for Environmental Engineering Related To Buildings, Bath, 1986. p. 236-246.

[6] Awbi H.B. and Setrak A.A., Air Jet Interference Due to Ceiling-Mounted Obstacles, Proc. of the International conference on Air Distribution in ventilated spaces, Stockholm, 1987. p. 431-437.

[7] Awbi H.B., Application of Computational Fluid Dynamics in Room Ventilation, Building and environment, 1989. 241: p. 73-84.

[8] Murakami S., Kato S. and Suyama Y., Numerical study on diffusion field as affected by arrangement of supply and exhaust openings in conventional flow type clean room, ASHRAE Transaction, 1989. 100(2): p. 659-668.

[9] Chen Q., Moser A. and Huber A., Prediction of Buoyant, Turbulent Flow by a Low-Reynolds-Number k-□ Model, ASHRAE Trans., 1990. 96(1): p. 564-573.

[10] Nielsen P.V., Specification of a Two-Dimensional Test Case, International Energy Agency, Energy Conservation in Buildings and Community Systems, Annex 20: Air Flow Pattern Within Buildings, ISSN 0902-7513 R9040, 1990. p. 1-15.

[11] J Lage L., Bejan A. and Anderson R., Removal of Contaminant Generated by a Discrete Source in a Slot Ventilated Enclosure, Int. J. Heat Mass Transfer, 1992. 355: p. 1169-1180.
[12] JLage L., Bejan A. and Anderson R., Efficiency of Transient Contaminant Removal from a Slot Ventilated Enclosure, Int. J. Heat Mass Transfer, 1991. 3410: p. 2603-2615.
[13] Abe K., Kondoh T. and Nagano Y., A New Turbulence Model for Predicting Fluid Flow and Heat Transfer in Separating and Reattaching Flows-II. Thermal Field Calculations, Int. J. Heat Mass Transfer, 1995. 38(8): p. 1467-1481.
[14] Chen Q. and Jiang Z., Evaluation of air supply method in a classroom with a low ventilation rate, Proceedings of the Jacques Cartier Conference, Montreal, Canada, 1992. p. 23-29.
[15] Kato S. and Murakami S., Three-dimensional numerical simulation of turbulent airflows in ventilated room by means of 2-equation model, International Symposium on CFD, Tokyo, 1985. p. 560-571.
[16] Williams P.T., Baker A.J. and Kelso R.M., Numerical calculation of room air motion-part 2: the continuity constraint finite element method for three-dimensional incompressible thermal flows, ASHRAE transactions, 1994. 100I: p. 531-548.
[17] Williams P.T., Baker A.J. and Kelso R.M., Numerical calculation of room air motion-part 3: three-dimensional CFD simulation of a full scale room air experiment, ASHRAE transactions, 1994. 100I: p. 549-564.
[18] Hsu T.H., Hsu P.T. and How S.P., Mixed convection in a partially divided rectangular enclosure, Numerical heat transfer, 1997. Part A, 31: p. 655-683.
[19] Davidson L.and Nielsen P.V., A study of laminar backward facing step flow, Dept. of building technology and structural engineering, Aalborg University, Denmark, 1998. p. 41-43.
[20] Calmidi V.V. and Mahajan R.L., Mixed Convection over a Heated Horizontal Surface in a Partial Enclosure, Int. J. Heat and Fluid Flow, 1998. 19: p. 358-367.
[21] Hu S.C., Barber J.M. and Chuah Y.K., A CFD study for cold air distribution systems, ASHRAE transactions, 1999. Part 1: p. 614-627.
[22] Gladstone C. and Woods A., On the application of box models to particle-driven gravity currents, Journal of fluid mechanics, 2000. 416: p. 187-195.
[23] Gladstone C. and Woods A., On buoyancy driven natural ventilation of a room with a heated floor, Journal of fluid mechanics, 2001. 441: p. 293-314.
[24] Sinha S.L., Numerical simulation of room airflow, PhD thesis, IIT Kharagpur, 2000.
[25] Su M., Chen Q.and Chiang C.M, Comparison of different sub-grid scale models of large eddy simulation for indoor airflow modeling, Journal of Fluid Engineering, 2001. 123: p. 628-638.
[26] Svidt K., Bjerg B. and Nielsen T.D., Initial studies on virtual reality visualization of 3D airflow in ventilated livestock buildings, Conference on Chalmers AVR II and CONVR, 2001. P. 89-103.
[27] Xu W. and Chen Q., A two layer turbulence model for simulating indoor airflow part I. model development, Energy and building, 2001. 33: p. 613-625.
[28] Xu W. and Chen Q., A two-layer turbulence model for simulating indoor airflow part II. Applications, Energy and building, 2001. 33: 627-639.
[29] Einberg G.and Holmberg S., Particle removal efficiency in a numerical test room, 4th international symposium on HVAC, Beijing, China, 2003. p. 431-440.
[30] Kameel R. and Khalil E., Prediction of flow, turbulence, heat transfer and humidity patterns in operating theatres, IECEC-2004, 2004. p. 23-29.
[31] Sun Y. and Smith T.F., Airflow characteristics of a room with square cone diffusers, Building and environment, 2005. 40: p. 589-600.
[32] Lin Y.J.P. and Linden P.F., A model for under floor air distribution system, Energy and building, 2005. 37: p. 399-409.

[33] Lam C.K.G. and Bremhorst K., A modified form of the k-ε model for predicting wall turbulence. Transactions of the ASME, 1981. 103: p. 456-460.
[34] Patankar S.V., Numerical Heat Transfer and Fluid Flow, McGraw Hill, Washington, 1980.
[35] Tripathi B., Moulic S. G., Investigation of the buoyancy affected airflow patterns in the enclosure subjected at the different wall temperatures, Energy and Buildings, 2007. 39: p. 906-912.
[36] Tripathi B., Arora R.C. and Ghosh Moulic S., Buoyancy Effects on the Air Movement Inside a Room, Proceedings of the 31st *National conference on fluid mechanics & fluid power NCFMFP*, Jadavpur University, Kolkata, India, 2004. p. 805-811.
[37] Nielsen P.V., 1990, Specification of a Two-Dimensional Test Case, International Energy Agency, Energy Conservation in Buildings and Community Systems, Annex 20: Air Flow Pattern Within Buildings, ISSN 0902-7513 R9040, 1-15.